High-Winding-Number Zero-Energy Edge States in Rhombohedral-Stacked Su-Schrieffer-Heeger Multilayers

Feng Lu, Ao Zhou, Shujie Cheng, 2,1,* and Gao Xianlong 1,†

1 Department of Physics, Zhejiang Normal University, Jinhua 321004, China
2 Xingzhi College, Zhejiang Normal University, Lanxi 321100, China

We study the topological properties of rhombohedral-stacked N-layer Su-Schrieffer-Heeger networks with interlayer coupling. We find that these systems exhibit 2N-fold degenerate zero-energy edge states with winding number W=N, providing a direct route to high-winding-number topological phases where W equals the layer number. Using effective Hamiltonian theory and Zak phase calculations, we demonstrate that the winding number scales linearly with N through a layer-by-layer topological amplification mechanism. We introduce the Wigner entropy as a novel detection method for these edge states, showing that topological boundary states exhibit significantly enhanced Wigner entropy compared to bulk states. Our results establish rhombohedral stacking as a systematic approach for engineering high-winding-number topological insulators with potential applications in quantum information processing.

I. INTRODUCTION

Topological insulators, characterized by an insulating bulk and conducting boundary states, have revolutionized condensed-matter physics by uncovering novel quantum phenomena rooted in nontrivial band topology[1–5]. Among the diverse topological systems, the Su-Schrieffer-Heeger (SSH) model, proposed initially to describe charge density waves in polyacetylene serves as a paradigmatic one-dimensional (1D) topological platform[6]. Its core feature lies in the interplay between nearest-neighbor (ν) and next-nearest-neighbor (ω) hopping amplitudes: when $|\nu| \neq |\omega|$, the system exhibits a nontrivial topological phase characterized by zero-energy edge states, whose number is dictated by the winding number of the Bloch Hamiltonian, a \mathbb{Z}_2 -invariant for the standard SSH model[6, 7].

The SSH model's conceptual simplicity has motivated its extension into multi-dimensional and multilayered configurations [8–10]. This is driven by the fact that topological phenomena in low-dimensional systems often feature enhanced tunability and are more readily accessible in experiments [11–15]. For example, 2D SSH lattices are known to harbor higher-order topological phases characterized by corner-localized zero modes [16–18], and studies of stacked SSH bilayers have revealed interlayercoupled topological states that interpolate between 1D and 2D behaviors. However, most studies to date have focused on low-winding-number SSH phases. The systematic construction and characterization of high-windingnumber phases with $|W| \gg 2$ -which feature more intricate manifolds of zero-energy edge states-remain comparatively unexplored, despite their potential to host exotic quantum phenomena such as highly degenerate edge modes [19–21], fractional charge localization [22–24], and enhanced robustness against disorder [19, 20].

Multilayered stacking emerges as a promising strategy to engineer high-winding-number topological states, as interlayer coupling can modulate the band topology of individual layers and induce collective nontrivial phases that are absent in singlelayer systems. This approach echoes recent progress in topological heterostructures: for example, rhombohedral-stacked graphene multilayers, when coupled to a Haldane model layer, exhibit high Chern number quantum anomalous Hall (QAH) states with |C| = N + 1 (where N is the number of graphene layers) [25]. In these systems, interlayer hoppings break the degeneracy of higher-order Dirac points in bulk graphene, while topological proximity effects from Haldane layers open up bulk band gaps while preserving nontrivial boundary transport, illustrating how stackinginduced hybridization gives rise to Chern numbers beyond the singlelayer limit [25–29].

The rhombohedral-stacked structure, with its unique interlayer coupling, is an ideal platform for probing the dependence of topological properties on layer number. The linear amplification of topological invariants with layer count, observed in graphene multilayer systems, provides a novel design strategy, yet this important layertopology relationship has not been systematically investigated in the SSH model. As a paradigm model of one-dimensional topological systems, it is noted that the topological characteristics of the SSH model are characterized by the winding number W with $W \pm 1$ or W=0 corresponding to nontrivial or trivial topological phases. When the SSH model is extended to a multilayer structure, interlayer transitions will break the topological constraints of the singlelayer system and induce a richer range of winding number values [30]. A key question arises: does the winding number of a rhombohedralstacked SSH multilayer scale strictly with the number of layers N, analogous to the layer-dependent Chern numbers in graphene multilayers?

Regarding the topological characteristics of the SSH model, many experiments have been carried out to conduct experimental research on it. The theoretical pre-

^{*} chengsj@zjnu.edu.cn

[†] gaoxl@zjnu.edu.cn

diction of the SSH model was verified by measuring the Zak phase [14, 31–38], acoustic signal [32, 37], optical signal [14, 33, 34, 36] and electrical signal [35, 38]. With the development of quantum chromatography technology, the Wigner phase space method has gradually become an alternative approach for distinguishing different quantum states or different quantum phases. Topological phase transitions are also a type of quantum phase transition. As topological phase transitions constitute a class of quantum phase transitions, and according to the bulk-boundary correspondence, nontrivial topology is manifested in boundary states. The Wigner phase space method is precisely based on the quasi-probability distribution of quantum states in the phase space. From this perspective, the Wigner phase space method seems to be a feasible approach for detecting topological boundary states. Many mathematical methods can be used to convert the experimental data from optical homodyne tomography into the state's Wigner function [39], which makes it possible to experimentally measure the Wigner function directly [40–42]. Therefore, we will explore whether the Wigner phase space method can be used to find topologically nontrivial edge states from a series of quantum states.

II. THE RHOMBOHEDRAL-STACKED SSH MULTILAYER SYSTEM

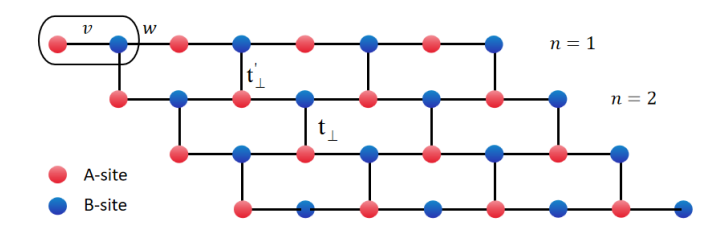


Figure 1. (Color online) Schematic illustration of the rhombohedral-stacked SSH multilayer system. Each unit cell (indicated by rounded rectangles) contains two sublattice sites: A (red) and B (blue). Within each SSH layer, the intra-cell and inter-cell hopping strengths are denoted by ν and ω , respectively. The interlayer coupling is characterized by two distinct hopping parameters: t'_{\perp} connects sublattice sites vertically between adjacent layers, while t_{\perp} provides the skewed interlayer connections that establish the rhombohedral stacking geometry.

The high winding number zero-energy topological states in this paper are engineered by spinless and non-interacting particles in an N-layer stacked system, which contains N SSH layers rhombohedral-stacked on each other, as shown in Fig. 1. The total Hamiltonian of this system is given by

$$\hat{H} = \sum_{n=1}^{N} \hat{H}_n + \sum_{n=2}^{N-1} \hat{H}_{n,n+1}^{\perp} + \hat{H}_{H}^{\perp}. \tag{1}$$

Each layer denotes the SSH Hamiltonian \hat{H}_n on a two-component superlattice [43], and it reads

$$\hat{H}_n = \sum_{j,n} \nu c_{j,A,n}^{\dagger} c_{j,B,n} + \omega c_{j,B,n}^{\dagger} c_{j+1,B,n} + \text{H.c.}, \quad (2)$$

where j is the super-cell index with A and B the sublattice sites, ν is the hopping strength within each super-cell, and ω is the hopping strength between nearest-neighbor super-cells. In experiments, the SSH model has been realized in the cold-atom optical lattice system [10, 36], acoustic system [32, 37], photonic crystal [44], and superconducting quantum circuit [38].

The Hamiltonian $H_{n,n+1}^{\perp}$ describing the interlayer hopping $(n \geq 2)$ is given by

$$\hat{H}_{n,n+1}^{\perp} = t_{\perp} \sum_{j} c_{j,B,n}^{\dagger} c_{j,A,n+1} + \text{H.c.},$$
 (3)

where t_{\perp} is the interlayer hopping strength. We consider the situation where the coupling between the first SSH layer and the remaining N-1 layer SSH network structure is weak and freely modulated $(t'_{\perp} \ll t_{\perp})$, whose Hamiltonian H_H^{\perp} is given by

$$H_H^{\perp} = t_{\perp}' \sum_{j} c_{j,B,0}^{\dagger} c_{j,A,1} + \text{H.c.}.$$
 (4)

When $t_{\perp}^{'}=0$, the 1D SSH model can be decoupled from this network structure.

Upon applying the Fourier transformation, we express the Hamiltonian in momentum space as

$$\hat{H} = \sum_{k} \psi_{k}^{\dagger} \mathcal{H}_{k} \psi_{k}, \tag{5}$$

where ψ_k represents the annihilation operator arranged as a column vector:

$$\psi_k = (c_{k,A,0} \ c_{k,B,0} \cdots \ c_{k,A,N} \ c_{k,B,N})^T.$$

Here, the subscripts denote momentum k, sublattice indices A and B, and layer number ranging from 0 to N. The corresponding Bloch Hamiltonian \mathcal{H}_k is a $2N \times 2N$ tridiagonal matrix:

$$\mathcal{H}_{k} = \begin{pmatrix} 0 & f_{k} & 0 & 0 & 0 & \cdots & 0 & 0 \\ f_{k}^{*} & 0 & t'_{\perp} & 0 & 0 & \cdots & 0 & 0 \\ 0 & t'_{\perp} & 0 & f_{k} & 0 & \cdots & 0 & 0 \\ 0 & 0 & f_{k}^{*} & 0 & t_{\perp} & \cdots & 0 & 0 \\ 0 & 0 & 0 & t_{\perp} & 0 & \cdots & 0 & 0 \\ \vdots & \vdots & \vdots & \vdots & \vdots & \ddots & \vdots & \vdots \\ 0 & 0 & 0 & 0 & 0 & \cdots & 0 & f_{k} \\ 0 & 0 & 0 & 0 & 0 & \cdots & f_{k}^{*} & 0 \end{pmatrix}, \tag{6}$$

where $f_k = \nu + \omega e^{-ik}$.

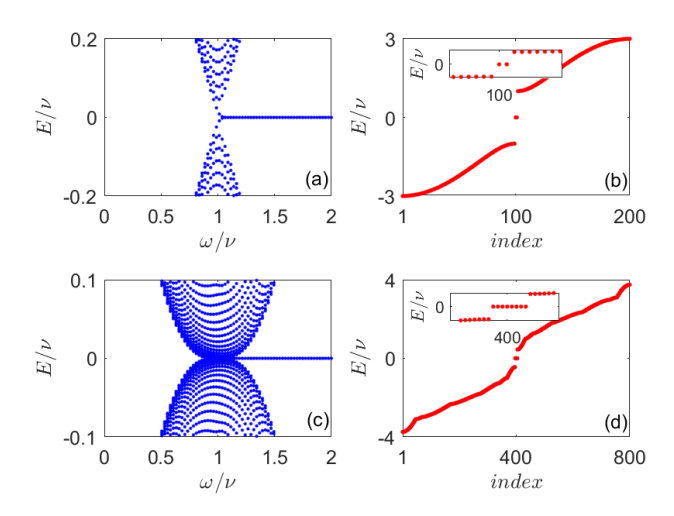


Figure 2. (Color online) (a) Band structure under N=1. (b) Energy versus energy level under N=1 and $\omega=2\nu$. (c) Band structure under N=5. (d) Energy versus energy level under N=5 and $\omega=2\nu$. Other involved parameters are $t'_{\perp}=0.1\nu,\,t_{\perp}=\nu$, and L=100.

III. ENERGY SPECTRUM AND WINDING NUMBER

The energy spectrum and eigenstates of the Hamiltonian in Eq. (6) can be obtained numerically via Schimidt orthogonalization. We firstly study the decoupling case with $t'_{\perp} = 0$. Under L = 100, the energy spectrum (lower and higher parts are not shown) as function of ω for the 1D SSH model (N=1) is plotted in Fig. 2(a). The zero-energy states are readily seen when $\omega > \nu$. Figure 2(b) shows the energy as a function of the energy level index for the $\omega = 2\nu$ case. It is seen from the inset that the zero-energy states have 2-fold degeneracy. Then we study the coupling case with $t'_{\perp} = 0.1\nu$. Taking N=4, the low-energy spectrum versus ω is plotted in Fig. 2(c). We can see that the zero-energy states exist when $\omega > \nu$ as well. Although these also are zero-energy states, we find that the degeneracy of the zero-energy state is closely related to the number of layers, presenting a 2N-fold degeneracy feature.

According to the bulk-edge correspondence [45], the winding number W corresponding to the 2-fold degenerate zero-energy states is W=1. Based on this, it can be inferred that that the winding number corresponding to the 2N-fold degenerate zero-energy state shall be W=N. For 2N-band Bloch systems, it is generally difficult to obtain the analytical solutions. But we can adopt effective methods to verify the numerical results. Employing the low-energy theory [46], the effective Hamiltonian of the rhombohedral-stacked (N-1)-layer SSH structure under $(c_{k,A,1}, c_{k,B,N})$ is given by

$$H_{N-1}^{SSH}(k) = \begin{pmatrix} 0 & F_{N-1}(k) \\ F_{N-1}^{*}(k) & 0 \end{pmatrix}, \tag{7}$$

with $F_{N-1}(k) = (-t_{\perp})^{2-N} f_k^N$, which is gapped system. When the first SSH layer is stacked on, the total effective Hamiltonian is given by

$$H_{\text{eff}}(k) = \begin{pmatrix} 0 & f_k & 0 & 0\\ f_k^* & 0 & t_{\perp}' & 0\\ 0 & t_{\perp}' & 0 & F_{N-1}(k)\\ 0 & 0 & F_{N-1}^*(k) & 0 \end{pmatrix}. \tag{8}$$

When an infinitesimal t'_{\perp} is turned on, the zero-energy states of the (N-1)-layer SSH system still locate in the band gap of the first-layer SSH model. As mentioned before, it is a fact that the singlelayer SSH model has 2-fold degenerate zero-energy states, leading to winding number W = 1. If the (N - 1) SSH multilayers system has winding number W = N - 1, the total winding number shall be W = N. Therefore, we transform the problem of proving that the winding number of this Nlayer stacked SSH system is W = N into proving that the winding number of the stacked (N-1)-layer SSH system is W = N - 1. Because an infinitesimal t'_{\perp} is introduced, the first layer SSH system can be regarded as no affected by the (N-1) SSH multilayers. The lowenergy subspace around the zero energy can by spanned by the basis $(c_{k,A,1} c_{k,B,N})$. The low-energy effective can be extracted from H(k) by the Schrieffer-Wolff transformation as

$$\begin{split} H_{N-1}^{\text{eff}}(k) &= H_{N-1}^{SSH} - SH_{SSH}^{-1} S^{\dagger} \\ &= \begin{pmatrix} 0 & F_{N-1}(k) \\ F_{N-1}^{*}(k) & 0 \end{pmatrix} - \begin{pmatrix} 0 & 0 \\ t'_{\perp} & 0 \end{pmatrix} \begin{pmatrix} 0 & f_{k} \\ f_{k}^{*} & 0 \end{pmatrix}^{-1} \begin{pmatrix} 0 & t'_{\perp} \\ 0 & 0 \end{pmatrix} \\ &= \begin{pmatrix} 0 & F_{N-1}(k) \\ F_{N-1}^{*}(k) & 0 \end{pmatrix}, \end{split}$$
(9)

where S and S^{\dagger} is the transformation operators, and H_{SSH} is the Hamiltonian of the singlelayer SSH model in momentum space.

We then analytically calculate the winding number. The Hamiltonian $H_{N-1}^{\mathrm{eff}}(k)$ scales as

$$H_{N-1}^{\text{eff}}(k) \propto \mathcal{H}_{N-1}^{\text{eff}}(k) = \begin{pmatrix} 0 & e^{-i(N-1)\phi(k)} \\ e^{i(N-1)\phi(k)} & 0 \end{pmatrix},$$
(10)

where $\phi(k) = \arctan\left(\frac{-\sin k}{\frac{\nu}{\omega} + \cos k}\right)$. The wave function $|u_{\pm}(k)\rangle$ of $\mathcal{H}_{N-1}^{\text{eff}}(k)$ is given by

$$|u_{\pm}(k)\rangle = \frac{1}{\sqrt{2}} \begin{pmatrix} e^{-i(N-1)\phi} \\ \pm 1 \end{pmatrix}, \tag{11}$$

where + and - corresponds to the positive and negative bands of $\mathcal{H}_{N-1}^{\text{eff}}(k)$, respectively. With $|u_{-}(k)\rangle$, the Zak phase [47] is given by

$$\phi_{\text{Zak}} = i \oint_{-\pi}^{\pi} dk \langle u_{-}(k) | \partial_{k} | u_{-}(k) \rangle$$

$$= \frac{1}{2} \oint_{-\pi}^{\pi} dk \frac{\partial \phi(k)}{\partial k}$$

$$= \begin{cases} 0, & \omega < \nu \\ (N-1)\pi, & \omega > \nu \end{cases}, \qquad (12)$$

from which we can extract the Winding number $W_{N-1}=\phi_{\rm Zak}/\pi=N-1$. Together with the first SSH layer, the whole winding number of the stacked N-layer SSH system is $W=W_{N-1}+1\equiv N$. This result is self-consistent with the 2N-fold degenerate zero energy states. It indicates that by designing a multilayer rhombohedral-stacked structure, high winding number zero-energy states can be achieved.

IV. WIGNER DISTRIBUTION AND WIGNER ENTROPY

Zero-energy states have been detected via Zak phase [14, 32–38], acoustic [32, 37], electrical [35, 38] and optical signals [14, 33, 34, 36]. We now propose an alternative detection method based on the Wigner distribution. The Wigner function W(x,p) in phase space for a wave function $|\psi\rangle$ is defined as [39–42]

$$W(x,p) = \frac{1}{2\pi\hbar} \int_{-\infty}^{\infty} \langle x - \frac{y}{2} | \rho | x + \frac{y}{2} \rangle e^{-\frac{ipy}{\hbar}} dy, \qquad (13)$$

where x and p denote the coordinate and momentum, respectively, and \hbar is the reduced Planck constant, and $\rho = |\psi\rangle\langle\psi|$. To analyze the boundary localization of zero-energy states, we preprocess the wave function by mapping the probability amplitudes from N layers to a single effective layer:

$$|\tilde{\psi}\rangle = \left[\phi_1 \ \phi_2 \ \cdots \ \phi_{L-1} \ \phi_L\right]^T,$$
 (14)

where the probability amplitude at site j is

$$\phi_{j} = \sum_{n=1}^{N} \frac{1}{N} \left[\varphi_{j,A,n}^{2} + \varphi_{j,B,n}^{2} \right], \tag{15}$$

with $\varphi_{j,A,n}$ and $\varphi_{j,B,n}$ being the original amplitudes. Normalization is not strictly necessary here. Substituting the preprocessed density matrix $\rho = |\tilde{\psi}\rangle\langle\tilde{\psi}|$ into Eq. (13) yields the Wigner distribution.

For parameters $t'_{\perp} = 0.1\nu$, $t_{\perp} = \nu$, N = 5, and L = 200, the Wigner distributions for the 1000-th eigenstate at $\omega = 1.5\nu$ (topological) and $\omega = 0.5\nu$ (trivial) are shown in Figs. 3(a) and 3(c) respectively. In the topological phase (Figs. 3(a)), W(x,p) exhibits boundary localization along the x-axis and a Gaussian distribution along the p-axis, characteristic of an edge state. In the

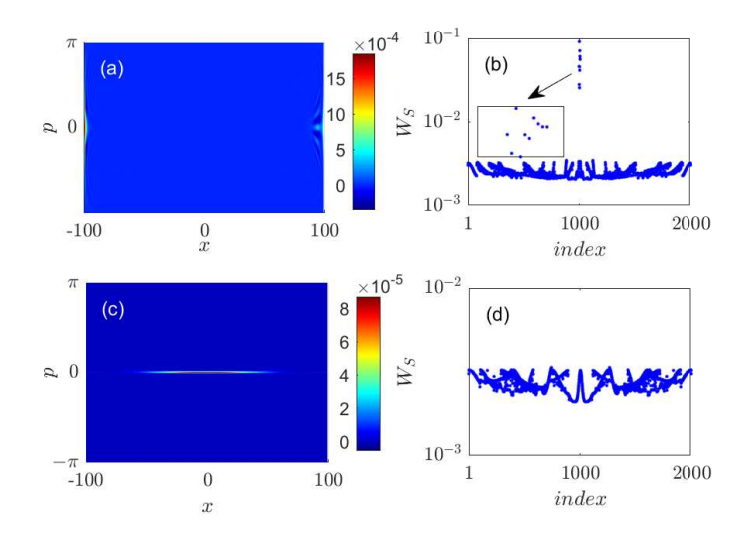


Figure 3. (Color online) Distinct signatures of topological edge states versus bulk states in Wigner phase space. (a) Wigner distribution W(x,p) for the 1000-th eigenstate in the topological phase ($\omega=1.5\nu$), showing pronounced spatial localization at the boundaries along the x-axis. (b) Corresponding Wigner entropy W_s as a function of energy level index, with significantly enhanced values for in-gap states (highlighted in inset), providing a clear phase-space diagnostic for topological edge states. (c), (d) Analogous results for the trivial phase ($\omega=0.5\nu$), where the Wigner distribution remains delocalized throughout the bulk (c) and the Wigner entropy maintains consistently low values across all states (d). The other parameters used are $t'_{\perp}=0.1\nu, t_{\perp}=\nu, N=5$, and L=200.

trivial phase (Figs. 3(c)), the distribution is Gaussian in x and discrete in p, indicating a bulk state. Manually inspecting Wigner distributions for each state is impractical. We therefore introduce a global quantity, the Wigner entropy, to distinguish edge states from bulk states, and it is defined as

$$W_s = -\int \int W(x, p) \ln |W(x, p)| dx dp, \qquad (16)$$

it quantifies the delocalization in phase space. Fig. 3(b) and Fig. 3(d) plot W_S versus energy level index for $\omega=1.5\nu$ and $\omega=0.5\nu$, respectively. The Wigner entropy of the zero-energy edge states is significantly larger than that of bulk states, providing a clear signature for identifying topological boundary states from the eigenstate spectrum.

V. SUMMARY

We have demonstrated that rhombohedral-stacked N-layer SSH systems host 2N-fold degenerate zero-energy edge states with winding number W=N. Through effective Hamiltonian analysis, we proved that weak interlayer coupling $(t'_{\perp} \ll t_{\perp})$ between the first SSH layer and the remaining (N-1)-layer network preserves the

topological properties while enabling linear scaling of the winding number with layer number. The Zak phase calculation confirms W=N in the topologically nontrivial regime $(\omega>\nu)$. The introduction of Wigner entropy as a diagnostic tool offers a new phase-space perspective for identifying topological boundary states. The enhanced Wigner entropy of edge states compared to bulk states provides a clear signature that complements traditional detection methods. This phase space approach may prove particularly valuable for experimental characterization of topological states in systems where conventional measurements are challenging.

Our key findings are: (i) The winding number scales exactly as W=N, establishing a one-to-one correspondence between layer number and topological invariant; (ii) The 2N-fold degeneracy of zero-energy states is protected by the rhombohedral stacking geometry; (iii) The Wigner entropy provides a robust experimental signature for detecting topological edge states, with bound-

ary states showing markedly enhanced entropy compared to bulk states in phase space. These results extend the layer-dependent topological amplification observed in graphene multilayers to one-dimensional systems, demonstrating that rhombohedral stacking is a universal strategy for engineering high-winding-number phases. The highly degenerate edge states may serve as a platform for topological quantum computation and the exploration of fractional charge localization in higher-winding-number regimes.

ACKNOWLEDGMENTS

This work is supported by the Natural Science Foundation of Zhejiang Province (Grants No. LQN25A040012), the start-up fund from Xingzhi College, Zhejiang Normal University, and the National Natural Science Foundation of China (Grants No. 12174346).

- M. Z. Hasan and C. L. Kane, Colloquium: Topological insulators, Rev. Mod. Phys. 82, 3045 (2010).
- [2] S.-Q. Shen, Topological Insulators: Dirac Equation in Condensed Matters, 2nd ed. (Springer, Singapore, 2017) p. 282.
- [3] C.-X. Liu, S.-C. Zhang, and X.-L. Qi, The quantum anomalous hall effect: Theory and experiment, Annual Review of Condensed Matter Physics 7, 301 (2016).
- [4] C.-Z. Chang, C.-X. Liu, and A. H. MacDonald, Colloquium: Quantum anomalous hall effect, Reviews of Modern Physics 95, 011002 (2023).
- [5] D. J. Thouless, M. Kohmoto, M. P. Nightingale, and M. den Nijs, Quantized hall conductance in a twodimensional periodic potential, Physical Review Letters 49, 405 (1982).
- [6] W.-P. Su, J. R. Schrieffer, and A. J. Heeger, Solitons in polyacetylene, Physical Review Letters 42, 1698 (1979).
- [7] S. A. Kivelson, A. J. Heeger, and J. R. Schrieffer, Solitons, polarons, and bipolarons in conducting polymers, Reviews of Modern Physics 59, 845 (1987).
- [8] P. Rosenberg and E. Manousakis, Topological superconductivity in a two-dimensional weyl ssh model, Phys. Rev. B 106, 054511 (2022).
- [9] F. Liu, Analytic solution of the n-dimensional suschrieffer-heeger model, Phys. Rev. B 108, 245140 (2023).
- [10] X. Zhou, J.-S. Pan, and S. Jia, Exploring interacting topological insulator in the extended su-schrieffer-heeger model, Phys. Rev. B 107, 054105 (2023).
- [11] D.-W. Wang, R.-B. Liu, S.-Y. Zhu, and M. O. Scully, Superradiance lattice, Phys. Rev. Lett. 114, 043602 (2015).
- [12] D.-W. Wang, H. Cai, L. Yuan, S.-Y. Zhu, and R.-B. Liu, Topological phase transitions in superradiance lattices, Optica 2, 712 (2015).
- [13] D. Obana, F. Liu, and K. Wakabayashi, Topological edge states in the su-schrieffer-heeger model, Phys. Rev. B 100, 075437 (2019).
- [14] G. Cáceres-Aravena, B. Real, D. Guzmán-Silva, A. Amo, L. E. F. Foa Torres, and R. A. Vicencio, Experimental

- observation of edge states in ssh-stub photonic lattices, Phys. Rev. Res. 4, 013185 (2022).
- [15] D. A. Khudaiberdiev, Z. D. Kvon, M. S. Ryzhkov, D. A. Kozlov, N. N. Mikhailov, and A. Pimenov, Twodimensional topological anderson insulator in a hgtebased semimetal, Phys. Rev. Res. 7, L022033 (2025).
- [16] F. Liu and K. Wakabayashi, Novel topological phase with a zero berry curvature, Phys. Rev. Lett. 118, 076803 (2017).
- [17] L. Trifunovic and P. W. Brouwer, Higher-order bulk-boundary correspondence for topological crystalline phases, Phys. Rev. X 9, 011012 (2019).
- [18] X.-J. Luo, X.-H. Pan, C.-X. Liu, and X. Liu, Higher-order topological phases emerging from su-schrieffer-heeger stacking, Phys. Rev. B 107, 045118 (2023).
- [19] E. G. Cinnirella, A. Nava, G. Campagnano, and D. Giuliano, Fate of high winding number topological phases in the disordered extended su-schrieffer-heeger model, Phys. Rev. B 109, 035114 (2024).
- [20] E. Di Salvo, A. Moustaj, C. Xu, L. Fritz, A. K. Mitchell, C. M. Smith, and D. Schuricht, Topological phases of the interacting su-schrieffer-heeger model: An analytical study, Phys. Rev. B 110, 165145 (2024).
- [21] A. Anastasiadis, G. Styliaris, R. Chaunsali, G. Theocharis, and F. K. Diakonos, Bulk-edge correspondence in the trimer su-schrieffer-heeger model, Phys. Rev. B 106, 085109 (2022).
- [22] Y. Wu, Fractional charges in the su-schrieffer-heeger model, (2022).
- [23] C. L. Kane and E. J. Mele, Quantum spin hall effect in graphene, Phys. Rev. Lett. 95, 226801 (2005).
- W. [24]A. Benalcazar, В. A. Bernevig, Quantized multi-Τ. Hughes, electric L. insulators, Science **357**, 61 (2017),pole https://www.science.org/doi/pdf/10.1126/science.aah6442
- [25] Y. Zhao, L. Zhang, and F.-C. Zhang, High chern number quantum anomalous hall states in haldane-graphene multilayers, [Submitted] (2025), document: LE20304B.pdf.
- [26] Y. Sha, T. Han, Z. Liu, et al., Observation of a chern in-

- sulator in crystalline abca-tetralayer graphene with spinorbit coupling, Science **384**, 414 (2024).
- Z. Lu, Y. Yao, J. Yang, [27] T. Han, J. Seo. K. Watanabe, T. Taniguchi, C. Yoon, L. Fu, F. Zhang, and L. Ju, Large quantum anomalous hall effect in spin-orbit proximitized rhombohedral graphene, Science **384**, 647 (2024),https://www.science.org/doi/pdf/10.1126/science.adk9749.
- [28] J.-H. Guan, W.-K. Lou, and K. Chang, Topological hidden phase transition in honeycomb bilayers with a high chern number, Physical Review B 110, 165303 (2024).
- [29] Z. Liu and J. Wang, Layer-dependent quantum anomalous hall effect in rhombohedral graphene, Physical Review B 111, L081111 (2025).
- [30] C.-S. Lee, I.-F. Io, and H. chung Kao, Winding number and zak phase in multi-band ssh models, Chinese Journal of Physics 78, 96 (2022).
- [31] Z.-X. Chen, Y.-H. Zhang, X.-C. Sun, R.-Y. Zhang, J.-S. Tang, X. Yang, X.-F. Zhu, and Y.-Q. Lu, Direct measurement of topological invariants through temporal adiabatic evolution of bulk states in the synthetic brillouin zone, Phys. Rev. Lett. 134, 136601 (2025).
- [32] M. Xiao, Z. Q. Zhang, and C. T. Chan, Surface impedance and bulk band geometric phases in onedimensional systems, Phys. Rev. X 4, 021017 (2014).
- [33] Z.-Q. Jiao, S. Longhi, X.-W. Wang, J. Gao, W.-H. Zhou, Y. Wang, Y.-X. Fu, L. Wang, R.-J. Ren, L.-F. Qiao, and X.-M. Jin, Experimentally detecting quantized zak phases without chiral symmetry in photonic lattices, Phys. Rev. Lett. 127, 147401 (2021).
- [34] Q. Wang, M. Xiao, H. Liu, S. Zhu, and C. T. Chan, Measurement of the zak phase of photonic bands through the interface states of a metasurface/photonic crystal, Phys. Rev. B 93, 041415 (2016).
- [35] K.-F. Luo and R. Yu, Topological states in electric circuit, Acta Phys. Sin. 68, 220305 (2019).
- [36] M. Atala, M. Aidelsburger, J. T. Barreiro, D. Abanin,

- and I. Bloch, Direct measurement of the zak phase in topological bloch bands, Nature Physics 9, 795 (2013).
- [37] M. Xiao, G. Ma, Z. Yang, P. Sheng, Z. Q. Zhang, and C. T. Chan, Geometric phase and band inversion in periodic acoustic systems, Nature Physics 11, 240 (2015).
- [38] F. Mei, G. Chen, L. Tian, S.-L. Zhu, and S. Jia, Topology-dependent quantum dynamics and entanglement-dependent topological pumping in superconducting qubit chains, Phys. Rev. A 98, 032323 (2018).
- [39] A. I. Lvovsky and M. G. Raymer, Continuous-variable optical quantum-state tomography, Rev. Mod. Phys. 81, 299 (2009).
- [40] T. Douce, A. Eckstein, S. P. Walborn, A. Z. Khoury, S. Ducci, A. Keller, T. Coudreau, and P. Milman, Direct measurement of the biphoton wigner function through two-photon interference, Sci. Rep. 3, 3530 (2013).
- [41] L. G. Lutterbach and L. Davidovich, Method for direct measurement of the wigner function in cavity qed and ion traps, Phys. Rev. Lett. 78, 2547 (1997).
- [42] K. Banaszek, C. Radzewicz, K. Wódkiewicz, and J. S. Krasiński, Direct measurement of the wigner function by photon counting, Phys. Rev. A 60, 674 (1999).
- [43] W. P. Su, J. R. Schrieffer, and A. J. Heeger, Solitons in polyacetylene, Phys. Rev. Lett. 42, 1698 (1979).
- [44] Z. Cui, M. Peng, X. Zhang, Q. Wei, M. Yan, and G. Chen, Realization of multiple topological boundary states in phononic crystals, Phys. Rev. B 107, 165414 (2023).
- [45] Y. Hatsugai, Chern number and edge states in the integer quantum hall effect, Phys. Rev. Lett. 71, 3697 (1993).
- [46] M. Koshino and E. McCann, Trigonal warping and berry's phase $N\pi$ in ABC-stacked multilayer graphene, Phys. Rev. B **80**, 165409 (2009).
- [47] J. Zak, Berry's phase for energy bands in solids, Phys. Rev. Lett. 62, 2747 (1989).